AIAA JOURNAL
Vol. 42, No. 1, January 2004

Driving Mechanisms of High-Speed Unsteady Spiked Body Flows, Part 2: Oscillation Mode

Daniel Feszty,* Ken J. Badcock,† and Bryan E. Richards‡
University of Glasgow, Glasgow, Scotland G12 8QQ, United Kingdom

The driving mechanism of the unsteady flow mode oscillation, arising over spiked bodies, was analyzed by using computational fluid dynamics as a tool. Laminar, axisymmetric flow at Mach 6.00 and Reynolds number (based on the blunt-body diameter) of 0.13×10^4 was simulated by a spatially and temporally second-order-accurate finite volume method. The model geometry was a forward-facing cylinder of diameter D equipped with a spike of length $L/D = 2.00$. Verification and validation of the numerical method are followed by a detailed analysis of the numerical results. It was found that, apart from some minor modifications, the oscillation flow mode was driven by the energetic shear-layer hypothesis of Kenworthy (Kenworthy, M., "A Study of Unstable Axisymmetric Separation in High Speed Flows," Ph.D. Dissertation, Dept. of Aerospace and Ocean Engineering, Virginia Polytechnic Inst. and State Univ., Blacksburg, VA, 1978), a viscous phenomenon in nature.

Nomenclature

a	=	nondimensional speed of sound a^*/u^*_∞
D	=	nondimensional blunt-body diameter D^*/D^*
d	=	diameter of the location of pressure measurement points
L	=	nondimensional spike length L^*/D^*
M	=	Mach number
p	=	nondimensional pressure $p^*/\rho^*_\infty u^{*2}_\infty$
p_{t2}	=	nondimensional pitot pressure
p_1	=	nondimensional static pressure
Re	=	Reynolds number based on blunt-body diameter
Sr	=	Strouhal number, $f^* u^*_\infty / D^*$
t	=	nondimensional time $t^*(u^*_\infty/D^*)$
v	=	nondimensional velocity u^*/u^*_∞
α	=	angle of incidence, deg
β	=	shock angle, deg
Δp	=	pressure amplitude

Subscripts and Superscripts

∞	=	freestream values
$*$	=	dimensional quantities

Introduction

THE occurrence, importance, and characteristic features of high-speed unsteady spiked body flows were reviewed in Ref. 1, where it was pointed out that such flows can appear in two very distinct flow modes: oscillation and pulsation. It was highlighted that the driving mechanisms of these flows are yet to be fully understood mainly because of the limitations of the experimental techniques used for their analysis. Therefore, the research performed at the University of Glasgow focused on the use of computational fluid dynamics (CFD) as a tool for the investigation of unsteady spiked body flows. Although a brief review of the overall research program has been given in Ref. 2, the present paper will focus on the detailed analysis of one of the flow modes, oscillation only. For the oscillation only one complete hypothesis has been suggested in the past, originating from Kenworthy.[3] The reason for this lies in the oscillation mode being typical of much higher freestreams than pulsation and also in its character of appearing in a less violent manner, exhibiting pressure amplitudes on the afterbody an order of magnitude smaller than for pulsation. Hence, this flow mode has not been recognized until the studies of Wood[4] and Holden,[5] and even after that it received considerably less attention than its more dramatic counterpart.

The test case to be analyzed in the present paper was chosen from the experimental work of Kenworthy.[3] The model geometry was a forward-facing cylinder equipped with a spike of the length of $L/D = 2.00$ (Fig. 1). Mach 6.00 freestream was considered with the Reynolds number based on the blunt-body diameter of 0.13×10^6. The flow was axisymmetric at zero angle of incidence. There were two pressure transducers placed at a diameter of $D/2$ on the face of the cylinder in the experiment, and the pressure was recorded at these points in the numerical method too.

CFD Approach

Grid Generation

Because of the axisymmetry of the problem, it was sufficient to model the body in a two-dimensional plane. A structured multiblock grid consisting of 140,000 cells in nine blocks was generated. The first spacing near the wall was $5 \times 10^{-5} \times D$ in both the streamwise and cross-sectional directions.

Numerical Method

The PMB code[6] was used for the numerical simulations. This is a generic CFD code developed at the University of Glasgow, employing a second-order cell-centered finite volume discretization method to solve the Navier–Stokes equations in two-dimensional, axisymmetric or three-dimensional fashion. In the present work axisymmetric laminar simulations were performed. Roe's scheme, involving Harten's entropy fix,[7] with MUSCL variable interpolation is used to discretize the convective terms and central differencing for the diffusive ones, leading to a spatially second-order-accurate discretization scheme. A steady-state calculation proceeds in two phases: the freestream starting solution is initially smoothed using an explicit scheme, and then an implicit scheme is employed to obtain rapid convergence. The linear system arising at each implicit time step is solved by using the generalized conjugate gradient method along with a BILU (block incomplete lower–upper)(0) factorization as a preconditioner. An important feature of the code is the use of approximate Jacobian matrices for the left-hand side of the linear system. The unsteady part of the code is second-order accurate in time and employs an implicit unfactored dual-time method.

Received 11 March 2002; revision received 10 July 2003; accepted for publication 12 August 2003.

*Research Assistant, Department of Aerospace Engineering; currently Assistant Professor, Department of Mechanical and Aerospace Engineering, Carleton University, 1125 Colonel By Drive, Ottawa, Ontario K1S 5B6, Canada. Member AIAA.

†Senior Lecturer, Department of Aerospace Engineering. Member AIAA.

‡Mechan Professor, Department of Aerospace Engineering. Associate Fellow AIAA.

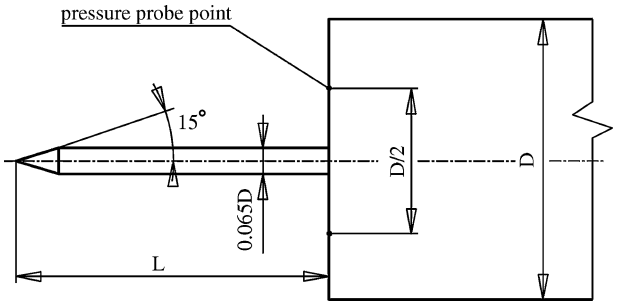

Fig. 1 Model geometry.

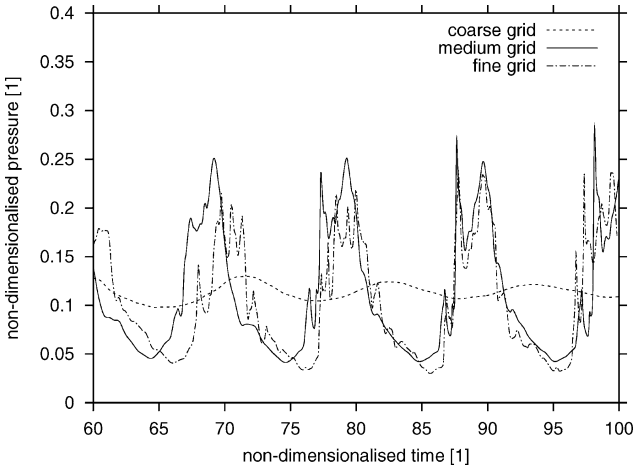

a) Grid-dependence tests

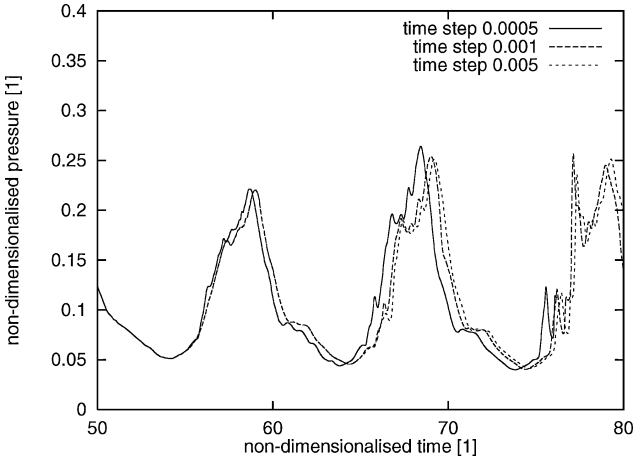

b) Time-step-dependence tests

Fig. 2 Results of numerical method's verification.

Results Verification

Three levels of grid density were considered for the grid-dependence tests. A medium grid and a coarse grid were extracted from the original fine mesh by taking every second and every fourth point, respectively, in each direction. Because of the different transients experienced on the various grid levels, the fine and the coarse grid histories were shifted along the time abscissa to allow easy comparison between the curves. The results are shown in Fig. 2a from which it is apparent that the resolution of the coarse grid is insufficient to develop proper unsteady flow. The pressure traces of the medium and fine grids, on the other hand, appear to agree well, yielding comparable pressure amplitudes and time periods. The graph shapes from these two grids also exhibit similarities, characterized by multiple peaks at the pressure maxima, and although the fine-grid results demonstrate some additional secondary peaks along the entire pressure trace the general trend of the two curves appear to agree and hence the medium grid can be selected for further analysis.

Table 1 Comparison of the time-averaged characteristics

Method	Δp	Sr
Experiment[3]	0.0745	0.1079
CFD	0.2693	0.0983

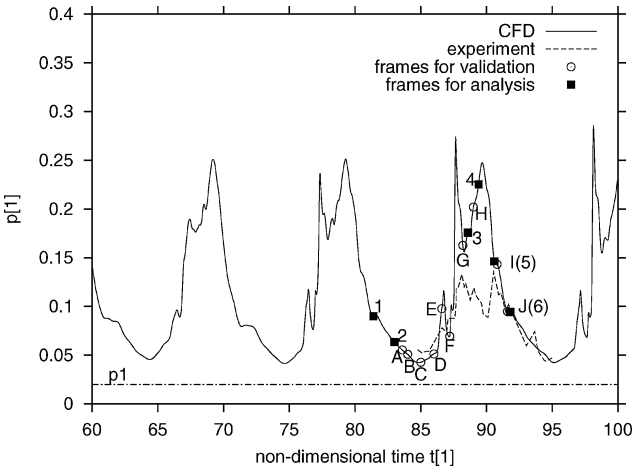

Fig. 3 Detail of the pressure history at the cylinder face ($d = D/2$) for the Mach 6.00 oscillation case ($L/D = 2.00$). The nondimensional value of p_{t2} is 0.9288.

The real time-step influence was also tested by decreasing the original 0.005 value by factors of 5 and 10 (Fig. 2b). Although the smaller time steps have the general effect of shifting the curves slightly forward along the time abscissa, the displacement is not significant, and hence the largest allowable time-step results can be used for further analyses.

Results Validation

The computational results were validated with the experimental data in terms of the time-averaged pressure amplitudes Δp, the time-averaged Strouhal numbers Sr, the characteristic shape of the pressure traces, and the shock envelope histories.

The cycles considered for the time averaging are shown in Fig. 3, along with a representative cycle from the experiment. It can be seen from this graph and also from Table 1 that although the pressure amplitude of the event is overpredicted by the simulation it can be still found of the order of 0.1, which is typical of oscillation.[3] The Strouhal numbers, on the other hand, appear to be in good agreement with the measured data. The characteristic feature of the pressure trace, the existence of multiple peaks at the pressure maxima, was also picked up by the CFD simulation. Although the magnitude of the discrepancy between the experiemantal and computational pressure amplitudes might question the validity of the numerical results, it was recently revealed by Kenworthy (private communication, 1999) that because of the possible errors in the experiment the amplitude of the pressure fluctuations should be treated more qualitatively than quantitatively. This was argued by the fact that in the experiment the pressure transducers were held in a cavity, which was likely to cause amplitude attenuation. Thus, the correct prediction of the Strouhal numbers and capturing the characteristic shape of the pressure trace appears to be far more important than the agreement of the amplitudes. Another factor contributing to the disagreement could be the difficulty of maintaining the axisymmetry at this long spike length in the experiment. These arguments are further substantiated by comparing the experimental and the numerical shock envelope histories (Fig. 4), showing good agreement. In this figure the CFD results are presented in terms of density isolines because these offer the best comparison to the density gradients captured on the shadowgraphs. The time positioning of the CFD frames is illustrated in the pressure trace shown in Fig. 3. As is evident, both the numerical and experimental shock envelopes

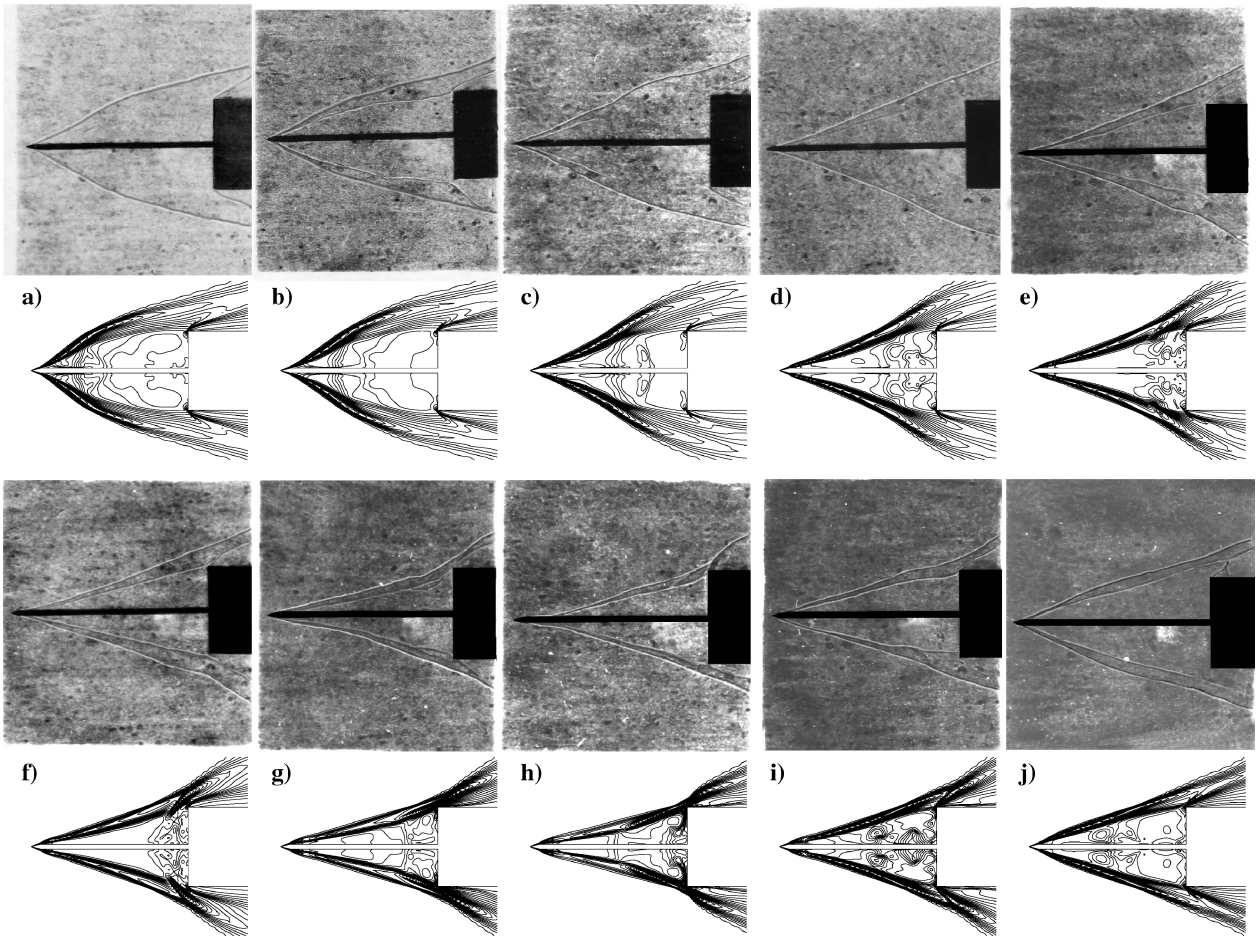

Fig. 4 Comparison of the shadowgraphs of Ref. 3 and the density isolines from the CFD for the frames indicated in Fig. 3.

are dominated by the shear layer's ever-changing shoulder reattachment condition, that is, its lateral "flapping" around the afterbody shoulder. The foreshock changes its shape as a consequence of this phenomena. It was suggested by Kenworthy[3] that at the shear layer's lowest (Figs. 4g and 4h) and highest (Figs. 4a–4d) positions mass influx or mass escape takes place, respectively. The excursion of the separation point along the spike as suggested by Holden[5] and Kenworthy[3] can also be observed from the CFD predictions.

Theoretical Analysis

The following analysis will be based around Kenworthy's energetic shear-layer hypothesis,[3] which suggests the oscillation to be driven by a constantly changing imbalance between two pressures: one supplied by the shear layer and termed as the potential reattachment pressure p_{rpot} and the one dictated by the geometry of the model shoulder, termed as the required reattachment pressure p_{rr}. Then, if 1) $p_{\text{rpot}} > p_{\text{rr}}$, then the particles in the dividing streamline (of the shear layer) are able to overcome the pressure rise at the afterbody shoulder and will pass downstream to yield mass escape from the separation zone, whereas if 2) $p_{\text{rpot}} < p_{\text{rr}}$, the particles in the dividing streamline are not able to overcome the pressure rise at the afterbody shoulder and will be reversed into the separation zone, yielding mass influx. Because the quantitative evaluation of these two terms could not be accomplished by measurement or analysis in the past,[3] they proved to be a major obstacle in the verification of Kenworthy's theory. However, their evaluation becomes possible by using CFD.

Required Reattachment Pressure

The required reattachment pressure represents the pressure experienced on the afterbody shoulder in a steady, shoulder reattaching separated flow. Shoulder reattachment, as illustrated in Fig. 5, is a complex situation, characterized by the partial reattachment of the shear layer and the appearance of compression and expansion waves around the shoulder.

While in a nonshoulder, or face, reattaching flow all streamlines of the shear layer impact on the model face, in partial reattachment only those from below the dividing streamline will do so. The dividing streamline is defined as the streamline stagnating on the model face, and in a steady reattaching flow this forms the boundary between the reversed (lower) and downstream passing (upper) streamlines. In the case of a full, or face, reattachment, all these streamlines impact on the model face as a result of the stagnation point being relatively too far from the model shoulder. However, in a shoulder reattaching flow the stagnation point is found just below the model shoulder, and hence the streamlines from above the dividing streamline will not impact on the model face but will pass downstream through a ray of expansion waves. The low pressure in this expansion will then communicate upstream via the boundary layer and yield a much lower pressure at the stagnation point p_x than in a nonshoulder, that is, face, reattaching flow (p_i, see Fig. 5b).

Although there were some approximate methods developed for the evaluation of p_i, which is in fact the upper bound of p_x, there are no universal tools available for the estimation of p_x. Kenworthy[3] proposed p_x to be constant for a given afterbody geometry yielding detached shock wave and, by using a combined experimental-analytical approach, even attempted to estimate its value for a forward-facing cylinder (i.e., the afterbody geometry of the present paper) as $p_x = 0.22 p_{t2}$.

This value can now be verified from the CFD analysis by considering the flow conditions of the Mach 6.00 oscillation but with $L/D = 2.75$ spike length, that is, the geometrical configuration nearest to the examined $L/D = 2.00$ case yielding steady separation. The results are shown in Fig. 6. The flow details and the surface-pressure distribution appears to agree qualitatively with the theoretical

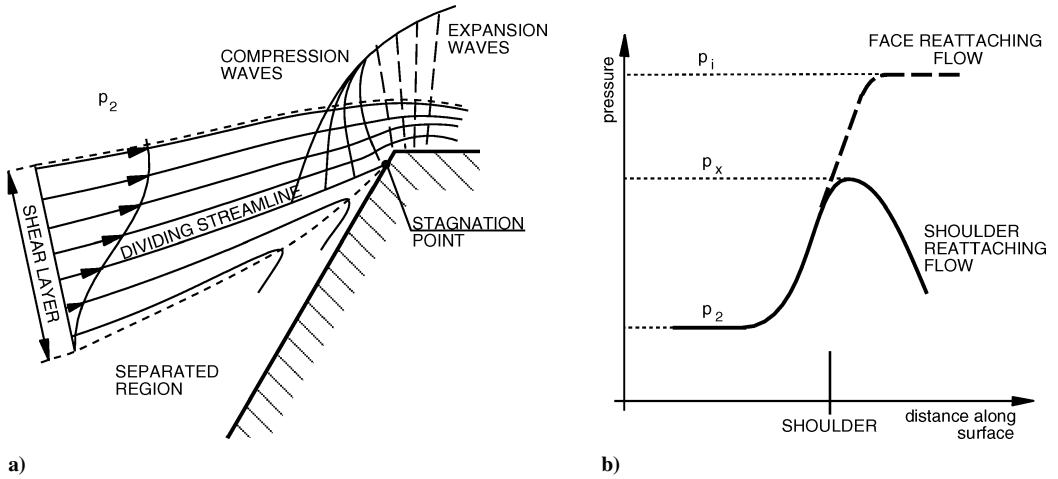

Fig. 5 a) Shoulder reattachment after Wood[4] and b) the corresponding surface pressure distribution according to Kenworthy.[3]

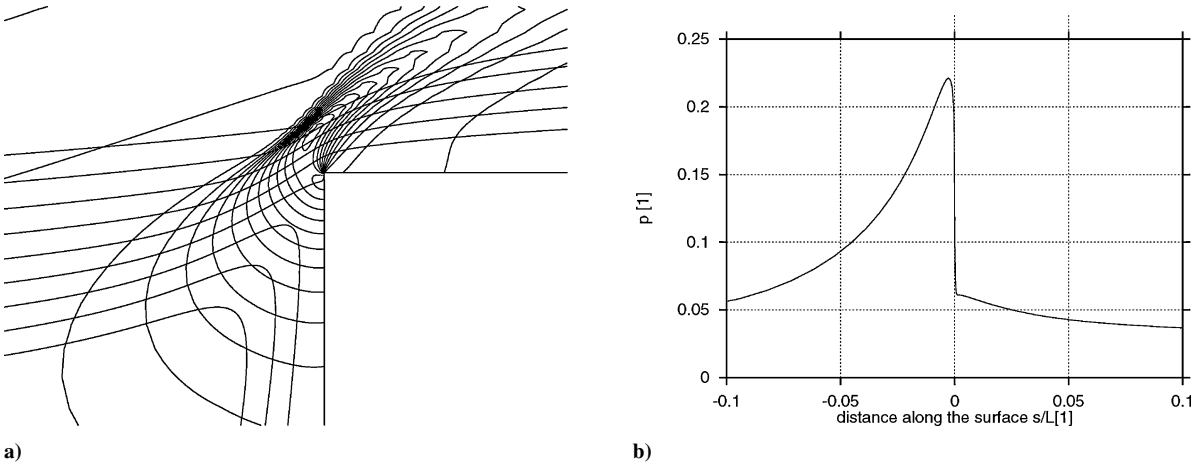

Fig. 6 CFD results of the shoulder reattachment for a steady separation at $M = 6.00$, $Re_D = 0.13 \times 10^6$, $L/D = 2.75$: a) pressure contours superimposed with streamlines and b) surface-pressure distribution in the vicinity of the shoulder.

assumptions in Fig. 5. The value of p_x can be recovered from Fig. 6b (note that the 0 of the horizontal abscissa marks the body shoulder) as 0.22 in nondimensional terms, which would correspond to $0.236 p_{t2}$ (see Fig. 3 for the nondimensional value of p_{t2}), that is, in good agreement with Kenworthy's estimate. Hence, the nondimensional value of

$$p_{\text{rr}} = p_x = 0.22 \tag{1}$$

will be used for the required reattachment pressure in the following.

Potential Reattachment Pressure

Chapman[8] proposed that the pressure supplied by the shear layer p_{rpot} is equal to that achieved by an isentropic compression of the dividing streamline if it would be brought to rest on the blunt-body shoulder; hence the term potential reattachment pressure. Although this appears to be a very simplified model, Burggraf[9] showed by numerical techniques that this is indeed a valid assumption, and hence the following expression can be used for the evaluation of p_{rpot} in the present paper[3]:

$$p_{\text{rpot}} = p_{0j} - p_2\{1 + [(\gamma - 1)/2]M_j\}^{\gamma/(\gamma - 1)} \tag{2}$$

Here, p_{0^j} is the total pressure on the dividing streamline, p_2 is the static pressure above the shear layer (Fig. 5), and M_j is the Mach number on the dividing streamline.

Kenworthy[3] performed an analysis on the variation of the attached boundary-layer length x_1, the velocity ratio on the dividing streamline $z_j = M_j/M_2$, and the potential reattachment pressure p_{rpot}, depending on the spike length L/D. These calculations were performed for the freestream conditions of the current case and involved axisymmetric and laminar considerations as well. The result of this analysis is shown in Fig. 7, from which it is apparent that as x_1 decreases, L/D decreases too and z_j and p_{rpot} increase with decreasing L/D. Use will be made of this information later in the explanation of the energetic shear-layer hypothesis.

Bounding and Escape Streamlines

The term dividing streamline provides a valid description of the shear layer in the vicinity of the separation point and at the reattachment in a steady separated flow only. However, in the case of an unsteady separation, such as the oscillation, this definition will no longer stand because the shear layer is constantly changing its position, causing always different streamlines to reattach on the blunt-body face. Therefore, it appears necessary to introduce two new terms to account for the description of the shear layer either in the vicinity of the separation point or at the reattachment.[3,10]

The term bounding streamline will be used to describe the shear layer in the vicinity of the separation point. It will be defined as the streamline that bounds the flow entrained by the shear layer originating from the separation zone from that coming from upstream.

The term escape streamline, on the other hand, serves to describe the situation in the vicinity of the reattachment point. The escape streamline will be defined as the highest streamline impacting on the afterbody shoulder, that is, reattaching.

In the case of mass escape, the bounding streamline lies above the escape streamline (Fig. 8a), whereas at mass influx the opposite is

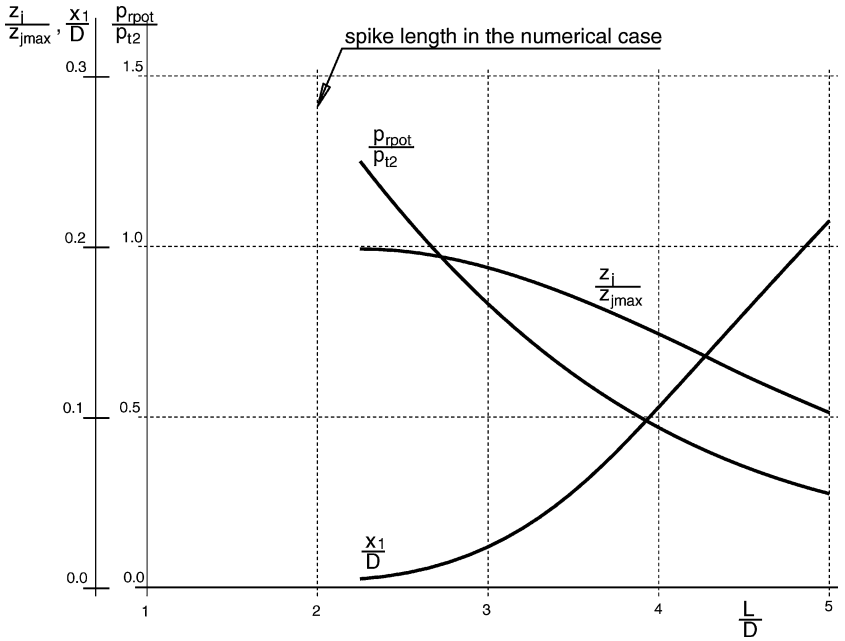

Fig. 7 Results of the free interaction calculation by Kenworthy[3]: $M = 6.00$ and $Re_D = 0.13 \times 10^6$ freestream considered.

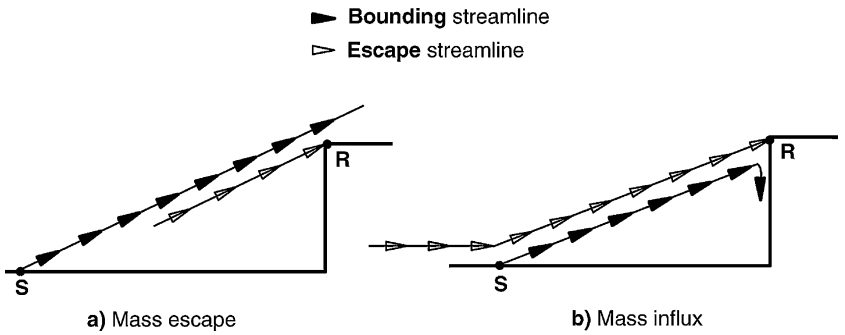

Fig. 8 Demonstration of the bounding and escape streamlines.

true (Fig. 8b). It is also clear from these definitions that the bounding streamline and the escape streamline coincide in steady separation, thus forming the classical dividing streamline.

Energetic Shear-Layer Hypothesis

Kenworthy's energetic shear-layer hypothesis[3] is introduced in the present section, along with a direct comparison to the results obtained from the numerical simulation ($M = 6.00$, $L/D = 2.00$).

The core of the hypothesis is shown in Fig. 9, in which the first column shows the original sketches of Kenworthy,[3] which were prepared solely on the basis of experimental observations and the concepts of the hypothesis. They depict the representative shape of the bounding streamline in five characteristic time instants. The magnitude of the streamline vectors indicate the magnitude of the local velocity.

The remaining columns show the results from the present simulation. First, the numerically obtained bounding streamlines are presented. These were created by launching a streamline from the separation point. Similar to Kenworthy's illustration, the magnitude of the dashes indicate the local velocity on the bounding streamline.

Next, the distribution of the Mach number M_j along the bounding streamline is provided, obtained again from the CFD results. These can be compared with the results in the second column and also serve as one of the inputs for the calculation of p_{rpot}.

Finally, the distribution of the potential reattachment pressure p_{rpot} along the bounding streamline is shown in the last column. This was calculated by using Eq. (2), where p_2 was substituted by the static pressure on the bounding streamline p_j (because $\partial p/\partial y = 0$ across the shear layer). The stagnation pressure on the bounding streamline p_{0j} is determined in Eq. (2) as[11]

$$p_{0j} = \frac{p_j}{\left(1 + M_j^2/5\right)^{-\gamma/(\gamma-1)}} \tag{3}$$

The analysis begins with frame 1 (Fig. 3), which is shown schematically in Fig. 9a. According to Kenworthy's sketch (first column), the velocity is fairly uniform and high along the bounding streamline . This is argued by the very small value of x_1, which implies a large z_j and p_{rpot} from Fig. 7.

It can be seen from the CFD results that all of these features are predicted by the numerical method. The velocity distribution along the bounding streamline is fairly uniform with M_j reaching values as high as 4. The potential reattachment pressure is also high ($p_{\text{rpot}} \gg p_{\text{rr}}$), although not as uniform as the velocity.

This configuration, that is, the bounding streamline lying above the escape streamline, yields mass escape from the separation zone. Thus, according to Kenworthy, after an interval of time required for this to be felt upstream, the separation recedes toward the model face (Fig. 9b). As x_1 increases, z_j and p_{rpot} will decrease as shown in Fig. 7. However, as the particles on the bounding streamline travel with a finite velocity between the separation and the reattachment, this effect will not be felt uniformly along the entire bounding streamline, but with a certain time lag. This means that, although the upstream part of the bounding streamline accommodates to the new p_{rpot} and M_j, the downstream one remains unaffected.

Once again, the CFD results agree very well with this part of the hypothesis. It is clearly demonstrated in the numerically obtained

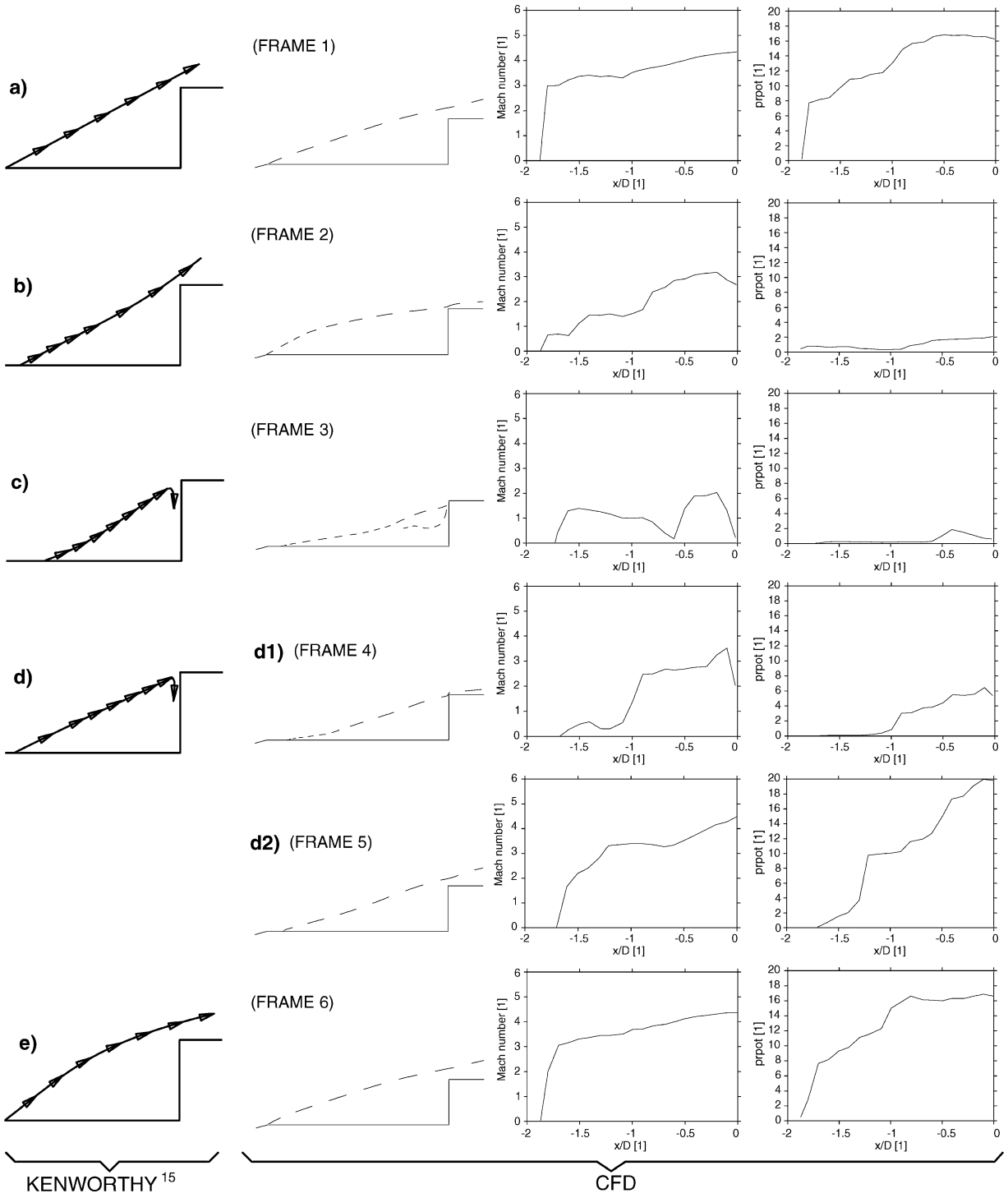

Fig. 9 Schematic of the energetic shear-layer hypothesis applied to $M = 6.00$, $L/D = 2.00$ case. First column shows Kenworthy's original sketches,[3] second column the corresponding bounding streamlines obtained by CFD (the frame numbers are from Fig. 3), and the third and the fourth columns show the Mach number and the potential reattachment pressure distributions along the bounding streamline.

bounding streamline that a smaller velocity appears near the separation, whereas a still larger one is present over the afterbody shoulder. The distribution of M_j further substantiates this trend. As a consequence, a small p_{rpot} is traveling downstream along the bounding streamline, while the value near the reattachment remains just high enough to maintain mass escape ($p_{\text{rpot}} > p_{\text{rr}}$).

Returning to Kenworthy's description, by Fig. 9c the last of the overenergetic fluid has passed downstream, and now the energy-deficient fluid is beginning to arrive to the reattachment region and is being reversed into the separation zone.

CFD shows a relatively small velocity along the entire length of the bounding streamline (see the magnitude of the dashes in the second column of Fig. 9c and the M_j distribution), which agrees well with the hypothesis. Also, a small p_{rpot} dominates the entire length of the streamline, with the value just in front of the cylinder face being approximately $\frac{1}{5}$ of that seen in the preceding frame. Hence, this will yield mass influx caused by $p_{\text{rpot}} < p_{\text{rr}}$.

Up until this point, Kenworthy's hypothesis and the CFD results were found in very good agreement. However, the first major difference could be observed in the comparison of Fig. 9d with the numerical results.

Kenworthy argued that after a certain time lag the separation point will react to the mass influx and be pushed forward toward the spike tip. By this, x_1 decreases, so that z_j and p_{rpot} will increase according

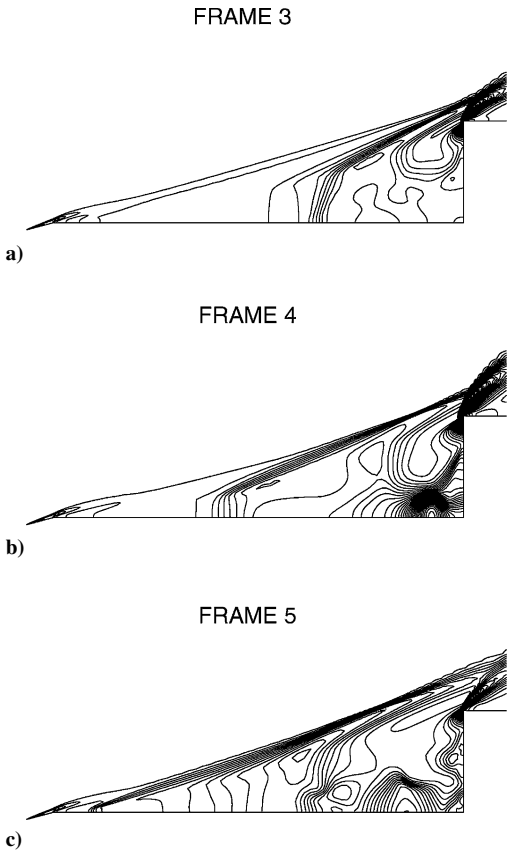

Fig. 10 Pressure isolines for frames 3,4, and 5 from Fig. 9.

to Fig. 7. This will be felt first at the separation point, and later, after the particles have traveled downstream, at the reattachment too. This would mean that larger velocity magnitudes would propagate in the downstream direction, that is, from the separation point toward the reattachment (see Fig. 9d).

The CFD results, however, show the sequence of the velocity change to occur in the opposite sense, that is, the larger velocity magnitudes appearing at the reattachment first and spreading upstream toward the separation point. This process is illustrated via two frames, Figs. 9d1 and 9d2. The same trend can be observed in the corresponding M_j and p_{rpot} plots: the larger Mach-number values (of the order of Mach 3) and the high pressure propagate upstream instead of downstream.

This phenomenon can be explained by the nature of pressure propagation within the separation zone. During the mass influx (Fig. 9c), the pressure builds up at the model face and starts to spread into the low-pressure separation zone. However, because of the zero pressure gradient through the shear layer ($\partial p/\partial y = 0$) this pressure propagation cannot occur in the separation zone only, but will affect both the shear layer and the supersonic flowfield behind the oblique shock wave. Hence, an upstream moving pressure wave, spanning from the spike surface to the oblique shock wave, is formed (see Fig. 10a showing the pressure isolines of frame 3 from Fig. 9). As this travels upstream (Figs. 10b and 10c), it alters the static pressure in the bounding streamline p_j along with M_j and p_{rpot}, too. This is felt first near the reattachment (Figs. 9d1 and 9d2) and then, once the high pressure is fully spread in the separated zone, at the point of separation too (Fig. 9e), which as a consequence of this moves forward to the spike tip.

The most important point, however, is that because of the increased p_{rpot} at the reattachment no mass influx can occur in Fig. 9d, but instead, mass escape will take place ($p_{\text{rpot}} > p_{\text{rr}}$). This is in contrast to Kenworthy's hypothesis.

Conclusions

The driving mechanism of the oscillation flow mode has been analyzed by using CFD as a tool. It was confirmed that this type of instability works according to Kenworthy's energetic shear-layer hypothesis. The unsteadiness is caused by the ever-changing shoulder reattachment condition, which occurs as a result of the mutual relationship of the pressure supplied by the shear layer p_{rpot} and the pressure dictated by the afterbody p_{rr}. The shear layer is lifted off from the afterbody shoulder when $p_{\text{rpot}} > p_{\text{rr}}$ and leads to mass escape from the separation zone, whereas it reattaches on the afterbody when $p_{\text{rpot}} < p_{\text{rr}}$ and causes mass influx into the separation zone. The conditions at the separation point react to this with a certain time lag, resulting in nonuniform distributions of the velocity and potential reattachment pressure along the shear layer.

The CFD results confirm Kenworthy's theory, apart from one minor modification regarding the propagation of pressure changes along the shear layer. It was found that a high pressure (in terms of p_{rpot}) and high velocity fluid can never precede a low pressure and low velocity fluid within the bounding streamline as it was thought in the past.

Oscillation, as a mode of unsteady spiked body flows, can be understood as a type of self-sustained oscillatory flows with impinging free shear layers. The present work showed that in this regard the ever-changing shoulder reattaching condition of the shear layer can be interpreted as the event of organized disturbance at the impingement, while the upstream propagation of the pressure wave within the separated region would correspond to the feedback signal in the self-sustained oscillation theory.

Acknowledgments

This work was supported by a University of Glasgow postgraduate scholarship and an Overseas Research Student Award from the Committee of Vice-Chancellors and Principals. The authors thank Michael A. Kenworthy for his comments on the numerical results.

References

[1]Feszty, D., Badcock, K. J., and Richards, B. E., "Driving Mechanisms of High-Speed Unsteady Spiked Body Flows, Part 1: Pulsation Mode," *AIAA Journal*, Vol. 42, No. 1, 2004, pp. 95–106.

[2]Feszty, D., Badcock, K., and Richards, B., "Utilising CFD in the Investigation of High-Speed Spiked Body Flows," *Aeronautical Journal*, Vol. 106, No. 1058, 2002, pp. 161–174.

[3]Kenworthy, M., "A Study of Unstable Axisymmetric Separation in High Speed Flows," Ph.D. Dissertation, Dept. of Aerospace and Ocean Engineering, Virginia Polytechnic Inst. and State Univ., Blacksburg, VA, 1978.

[4]Wood, C., "Hypersonic Flow over Spiked Cones," *Journal of Fluid Mechanics*, Vol. 12, No. 4, 1961, pp. 614–624.

[5]Holden, M., "Experimental Studies of Separated Flows at Hypersonic Speeds. Part 1—Separated Flows over Axisymmetric Spiked Bodies," *AIAA Journal*, Vol. 4, No. 4, 1966, pp. 22, 23.

[6]Badcock, K., Richards, B., and Woodgate, M., "Elements of Computational Fluid Dynamics on Block Structured Grids Using Implicit Solvers," *Progress in Aerospace Sciences*, Vol. 36, 2000, pp. 351–392.

[7]Gnoffo, P., "Point-Implicit Relaxation Strategies for Viscous Hypersonic Flows," *Computational Methods in Hypersonic Aerodynamics*, edited by T. K. S. Murthy, Kluwer Academic, Norwell, MA, 1993, pp. 115–151.

[8]Chapman, D., "Laminar Mixing of a Compressible Fluid," NACA TR 958, 1950.

[9]Burggraf, O., "Inviscid Reattachment of a Separated Shear Layer," *Proceedings of the 3rd International Conference on Numerical Methods in Fluid Mechanics*, Vol. 2, 1972.

[10]East, R., and Wilkinson, P., "A Study of the Oscillating Separated Flow Ahead of a Forward Facing Step Oscillating Traversely to a Hypersonic Free Stream," Southampton Univ., AASU Rept. 263, Southampton, England, U.K., Jan. 1966.

[11]"Equations, Tables, and Charts for Compressible Flow," NACA 1135, 1953.

M. Sichel
Associate Editor